Princeton Plasma Physics Laboratory

PPPL- 4734

PPPL- 4734

Plasma Equilibrium Reconstructions In The Lithium Tokamak Experiment

Laura Berzak Hopkins, J. Menard, R. Majeski, D.P. Lundberg, E. Granstedt,
C. Jacobsen, R. Kaita, T. Kozub and L. Zakharov

February, 2012

PPPL PRINCETON PLASMA PHYSICS LABORATORY

Prepared for the U.S. Department of Energy under Contract DE-AC02-09CH11466.

Princeton Plasma Physics Laboratory
Report Disclaimers

Full Legal Disclaimer

Trademark Disclaimer

PPPL Report Availability

Princeton Plasma Physics Laboratory:

http://www.pppl.gov/techreports.cfm

Office of Scientific and Technical Information (OSTI):

http://www.osti.gov/bridge

Related Links:

U.S. Department of Energy

Office of Scientific and Technical Information

Fusion Links

Plasma equilibrium reconstructions in the lithium tokamak experiment

L Berzak Hopkins, J Menard, R Majeski, D P Lundberg, E Granstedt, C Jacobsen, R Kaita, T Kozub, and L Zakharov

Princeton Plasma Physics Laboratory, Princeton University, Princeton, New Jersey 08543, USA
Suggested *PACS* code: 52.55.Fa (Tokamaks, spherical tokamaks)
Submitted to: Nuclear Fusion

Abstract.
The Lithium Tokamak Experiment (LTX) (R_0 = 0.4 m, a = 0.26 m is designed to explore the low-recycling, lithium wall operating regime for magnetically confined plasmas. A set of shell quadrants internal to the vacuum vessel and conformal to the plasma last closed flux surface is designed to be coated with lithium to produce the lithium plasma-facing surface. The shell quadrants are highly conductive in order to maintain an even thermal distribution, but this conductivity also permits eddy currents to flow that can be larger in magnitude than the plasma current. Due to this effect, plasma start-up is greatly complicated as is the development of an applicable equilibrium solver code. A suitable code, LTX LRDFIT, has been developed and benchmarked and has now been used to compare plasma flux surface reconstructions for discharges before and after initial lithium wall conditioning. Dramatic improvements in plasma performance and shaping have been noted with the introduction of lithium.

(Some figures may appear in colour only in the online journal)

1. Introduction

The Lithium Tokamak eXperiment (LTX) [1] is a modest sized, ohmically-driven, spherical tokamak (R_0 = 0.4 m, a = 0.26 m, $B_T \sim 0.2$ T) designed to investigate the low-recycling, lithium wall operating regime [2] and extend the promising results of the Current Drive Experiment-Upgrade (CDX-U) (R_0 = 0.34 m, a = 0.22 m, $B_T \sim 0.2$ T). During the CDX-U lithium campaign, CDX-U operated with a heated tray limiter load with liquid lithium. The limiter extended in the toroidal direction and had a radius of 34 cm, a width of 10 cm, and a depth of 0.5 cm and provided a liquid lithium surface area of 2000 cm^2 [3]. Utilizing the tray limiter, a 5-10 fold increase in fueling requirements was noted between pre- and post-lithium CDX-U discharges [4]. Furthermore, CDX-U observed a 6-fold increase in the energy confinement time, from 1 ms to 6 ms. This improvement in energy confinement time is the largest relative increase measured in an Ohmically-heated tokamak and exceeds the ITER98P(y,1) ELMy H-mode scaling by a factor of 2-3 [5].

In order to expand upon these results and investigate this regime, LTX has an inner liner, or shell, constructed of 1 cm-thick copper faced with 1.5 mm-thick 304 stainless steel, internal to the vacuum vessel (figure 1). The thin stainless steel layer protects the underlying copper from reacting with lithium. The shell structure can be heated to 300 °C and its plasma facing surface (the thin stainless steel layer) coated with lithium, producing a liquid lithium surface area of 5 m^2.

This shell structure is shaped to be conformal to the plasma last closed flux surface and is segmented into electrically isolated quadrants. This segmentation forms two toroidal shell gaps and both outboard and inboard poloidal gaps, yielding two upper shell halves and two lower halves, as can be seen in figure 1. The shell quadrants cover approximately 85% of the plasma last closed flux surface, leaving exposed only a 5 cm inboard poloidal gap, a 12.5 cm outboard poloidal gap, and two 22.5° toroidal breaks. These shell gaps allow diagnostic access to the plasma and prevent a toroidally continuous eddy current from flowing on the shell around the plasma.

The copper backing of the shell minimizes temperature variations over the plasma facing shell surface as the shells are heated, a key feature required for uniform lithium coatings. However, copper is also highly electrically conductive. Even with the segmentation of the shell structure, significant (tens of

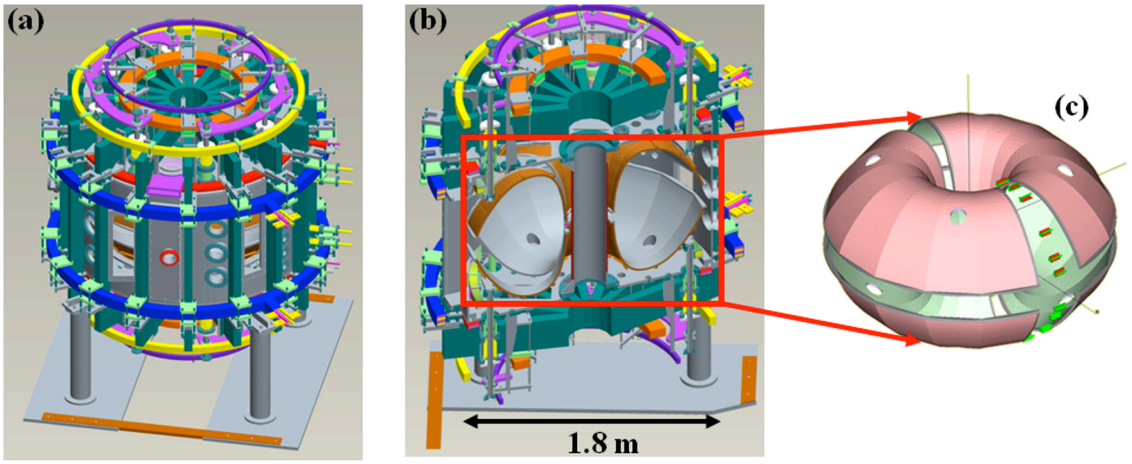

Figure 1 (Colour online): Images of (a) LTX outer vacuum vessel and field coils; (b) cutaway of LTX showing internal shell structure; (c) zoomed view of LTX shell quadrants with Mirnov coils (red/green) in a toroidal shell gap.

kiloamperes) eddy currents can and do circulate in each shell quadrant (figure 2) and, for the longest time constant component, require approximately 300 ms to decay to 1% of its initial magnitude [6]. The principal sources of these eddy currents are the changing currents in the Ohmic winding in the centerstack and in the largest set of poloidal field coils. Therefore, these eddy currents are present even during no-plasma vacuum field test shots. The primary eddy current structure is visualized in figure 2 and is seen to circulate toroidally and poloidally around each shell quadrant.

Because of their magnitude and duration, these non-axisymmetric, circulating eddy currents introduce significant challenges both to plasma start-up [7] and to the development of equilibrium solver codes suitable for reconstructing LTX plasmas. However, accurate reconstructions of LTX plasmas are essential for a full evaluation of the effect of the lithium wall on plasma performance. To meet this need, an extensive series of magnetic diagnostics were specifically designed and installed on LTX [8], and a suitable code (LTX LRDFIT) has been constructed for the unique LTX conducting system and is described more fully below. LTX LRDFIT was first utilized to develop reliable plasma start-up [6,7] and has now been utilized to calculate plasma reconstructions before and after initial lithium wall conditioning. Comparison of plasma reconstructions before and after lithium conditioning show dramatic performance enhancements with the introduction of lithium.

2. LTX LRDFIT description

The LRDFIT (LR circuit model with Data FITting capabilities) code was originally developed for use on the National Spherical Torus Experiment (NSTX) [9][1] and has now been adapted for use with the LTX magnetic diagnostics, vacuum vessel, and shell structure.

LRDFIT is a versatile code with the ability to calculate contour plots and magnetic field vectors in vacuum, in the plasma, and within conducting structures. LRDFIT can also simulate sensor responses

[1] The homepage for the LRDFIT code as utilized for NSTX is: http://w3.pppl.gov/~jmenard/software/lrdfit/lrdfit-index.htm

to field coil pulses and has the capability to accept user-defined field coil current waveforms as input and simulate the resulting sensor responses and field structure. This feature of LRDFIT is a critical capability for start-up and discharge design, which requires determining suitable coil current waveforms to yield the desired in-vessel field structure. As an equilibrium solver code, LRDFIT can reconstruct plasma fields using a plasma toroidal current density singular value decomposition (SVD) fit to measured data technique (with no force balance constraint).

LTX LRDFIT is an axisymmetric code which includes an LTX cross-sectional model that incorporates the vacuum vessel, field coils, shell quadrants, and plasma; each of these components is geometrically divided into distinct conducting regions. These conducting regions take the form of parallelograms,

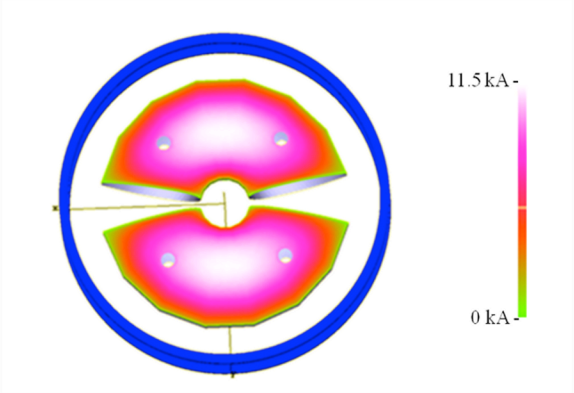

Figure 2 (Colour online): Three-dimensional simulation of eddy current density structure established in the upper shell quadrants by a square wave current pulse in the shown (dark blue) poloidal field coil set. Colour bar scale indicates magnitude of circulating current.

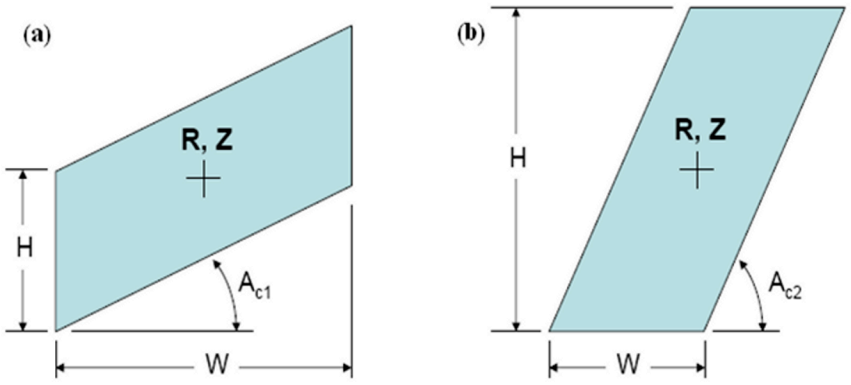

Figure 3: LRDFIT conducting regions – (a) One permissible orientation for a conducting region; (b) Second permissible orientation for a conducting region; only one angle (AC1 or AC2) can be defined per conducting region.

defined by a height, width, and angle (figure 3). The parallelogram regions are then subdivided into smaller rectangular conducting elements that conserve the parallelogram cross-sectional area. Each element has assigned inductance (L) and resistance (R) values which are used in the circuit equations linking the elements (equation 1):

Equation (1) $$M_{ij}(dI/dt)_j + R_i I_i = V_i$$

where M_{ij} is the mutual inductance between elements i and j; R_i is the resistance of element i, and I_i is the current in conducting element i.

Since LRDFIT is an axisymmetric code, each rectangular element is in actuality a rectangular cross-section ring. Therefore, the element resistance values, R_i, are given by $R_i = \eta_i\, 2\pi r_i/(w_i\, h_i)$, where r_i is the element mean radius, w_i is the element full width, h_i is the element full height, and η_i is the element resistivity. Inductance values are computed for each element based on numerical interpolation of published inductance tables. The self-inductance L for a circular coil of rectangular cross-section is given by $L = \mu_0 \pi r^2\, K\square\,(r,w,h) / h$ where $K\square$ is taken from Reference 10. The mutual inductance M_{ij} between two concentric, circular, single-turn coils with rectangular cross-sections centered at r_i,z_i and r_j,z_j with full widths w_i,w_j and full heights h_i,h_j is computed using formulae from Reference 11:

Equation (2)
$$\begin{aligned} M_{ij} = (\ & M_f(r_i,z_i,r_j+w_j/2,z_j)+M_f(r_i,z_i,r_j-w_j/2,z_j)+M_f(r_i,z_i,r_j,z_j+h_j/2)+M_f(r_i,z_i,r_j,z_j-h_j/2) \\ & +M_f(r_j,z_j,r_i+w_i/2,z_i)+M_f(r_j,z_j,r_i-w_i/2,z_i)+M_f(r_j,z_j,r_i,z_i+h_i/2)+M_f(r_j,z_j,r_i,z_i-h_i/2) \\ & - 2M_f(r_i,z_i,r_j,z_j)\ )/6 \end{aligned}$$

where $M_f(r_i,z_i,r_j,z_j)$is the mutual inductance between two current filaments centered at r_i,z_i and r_j,z_j respectively. The current, I, can have a time dependence and is treated as purely toroidal and axisymmetric within the element, while the associated current density is held constant.

The number of simultaneous equations is reduced by grouping elements with uniform resistivity into "passive" and "coil" regions. "Passive" regions include elements which do not have applied driving voltages, such as the elements comprising the vacuum vessel, shell, and plasma. "Coil" regions specify the field coil elements and contain driving voltages. The value of V_i is either 0 for "passive" regions or a time-dependent voltage for "coil" regions. The resulting circuit equations are diagonalized to retain explicitly all L/R time scales and are solved analytically by assuming linearly continuous driving voltages during each arbitrary time step.

For LTX LRDFIT, the LTX vacuum vessel and shell were divided into distinct conducting regions, 35 regions for the vacuum vessel and 42 regions each for the upper and lower shells (figure 4). During code calculations, these regions are subdivided into rectangular elements, and the field due to a distributed current across the rectangular cross-section conductor (element) is calculated. This distributed current treatment of conductors permits accurate calculation of field quantities near and inside the conductors themselves. Formulae for the flux and field from such a circular coil with a constant distributed current density are given by Reference 12 and involve slowly converging series of Legendre polynomials. To significantly reduce the computational time for the flux and field calculations, the leading order singular terms in the coil equations of Reference 12are expressed analytically, and the remaining smoothly varying terms are computed using numerical interpolation of tabulated values. These calculations are too lengthy to be repeated here and will be published separately.

Modeling the field magnitude near the actual conducting structures enables accurate modeling of the magnetic sensor response, which in turn allows the circulating eddy currents generated by the external field coils to be quantified. Accordingly, this modeling permits an interpretation of the eddy currents' effects on LTX plasmas. Because the eddy currents' magnitude can be larger than the pre-lithium plasma current, they have a significant effect on plasma behavior, and so it is critical that LRDFIT has the ability to incorporate eddy currents into the simulation.

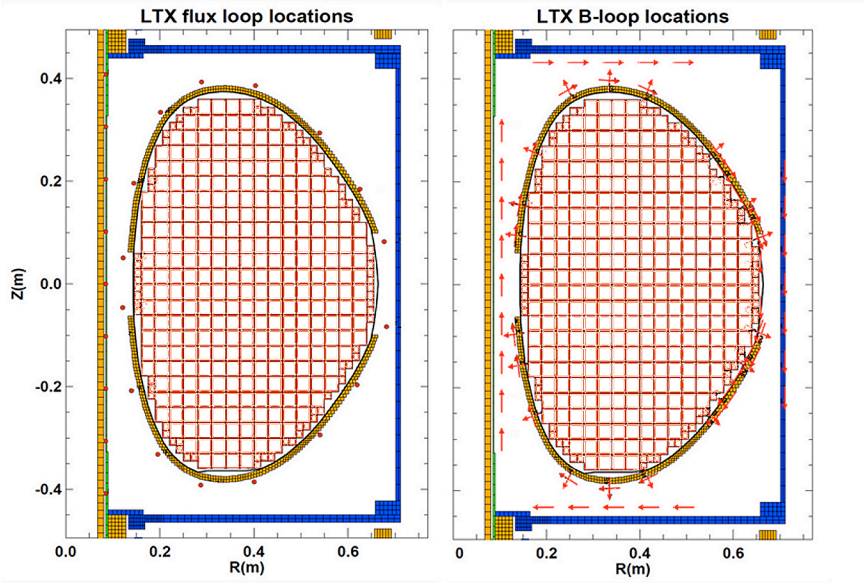

Figure 4: Diagrams indicating divisions of vacuum vessel, shell, and plasma volume into elements as well as placement of magnetic sensors in LTX LRDFIT – (a) Cross-sectional location of flux loops indicated by circles; (b) Cross-sectional location of Mirnov coils indicated by arrows. The rectangles outlined in red and enclosed by the limiter boundary (black line) are regions where the plasma toroidal current is allowed to flow in the LRDFIT model.

However, this ability alone is not suitable to model LTX plasmas. LRDFIT is an axisymmetric, and therefore inherently, two-dimensional code, while LTX is an inherently three-dimensional machine because of the structure of the shell quadrants. A true representation of the shell eddy current distribution requires n=0 as well as higher order, even (2n) Fourier components. LRDFIT, as an axisymmetric code, cannot incorporate n>0 components. Therefore, to apply the LRDFIT code to LTX plasmas, a suitable two-dimensional representation of the three-dimensional nature of LTX has been developed and implemented in LTX LRDFIT. This reduced representation allows the code to model specific effects of the three-dimensional nature of LTX without actually requiring a three-dimensional simulation [6].

Two key features of the LRDFIT circuit model are required to achieve this result. First, since the upper and lower conducting shells of LTX physically cannot support net toroidal current, the LRDFIT model must incorporate this constraint. To incorporate this constraint, each of the shells in the LTX LRDFIT model are connected to a fictitious (simulated model) power supply that controls the total simulated toroidal current of each shell such that the current is held at zero. Since the shell conducting elements are treated as parallel conductors in a single group connected to a power supply, different (including opposing) toroidal current densities are allowed to flow in the different parts of the shell in response to the spatially varying inductive voltage distribution within the shells.

Second, the LTX LRDFIT model of the conducting shells was further modified by introducing an empirical multiplier in the resistivity of shell elements (Equation 1), establishing a major radius dependence in the shell elements' resistivity. In this empirical approach, the shell element resistivity multiplier was specified at three major radial locations: R_{min}, R_{max}, and $R_{mid} = (R_{max}+R_{min})/2$ where R_{min} and R_{max} are the minimum and maximum radius values of the LTX conducting shells. The resistivity multiplier was then linearly interpolated as a function of R between R_{min} and R_{mid} and between R_{mid} and R_{max}. The resistivity multipliers used at each of the three locations were: 1, 2, 4, and 10 for a total of sixty-four different resistivity multiplier basis functions. Including this empirical resistivity factor can account for the increased path-length (and thus the effective resistance) for currents flowing in the actual,

physical shells, where actual current must flow poloidally at the toroidal ends of the shells due to the presence of the shell toroidal gaps. LRDFIT simulations were performed for individual poloidal field-only vacuum shots (no plasma) for each resistivity multiplier basis function. The optimal value of the empirical multiplier was then determined through a least squares minimization procedure, minimizing the error between measured and simulated data for the vacuum field pulses [6].

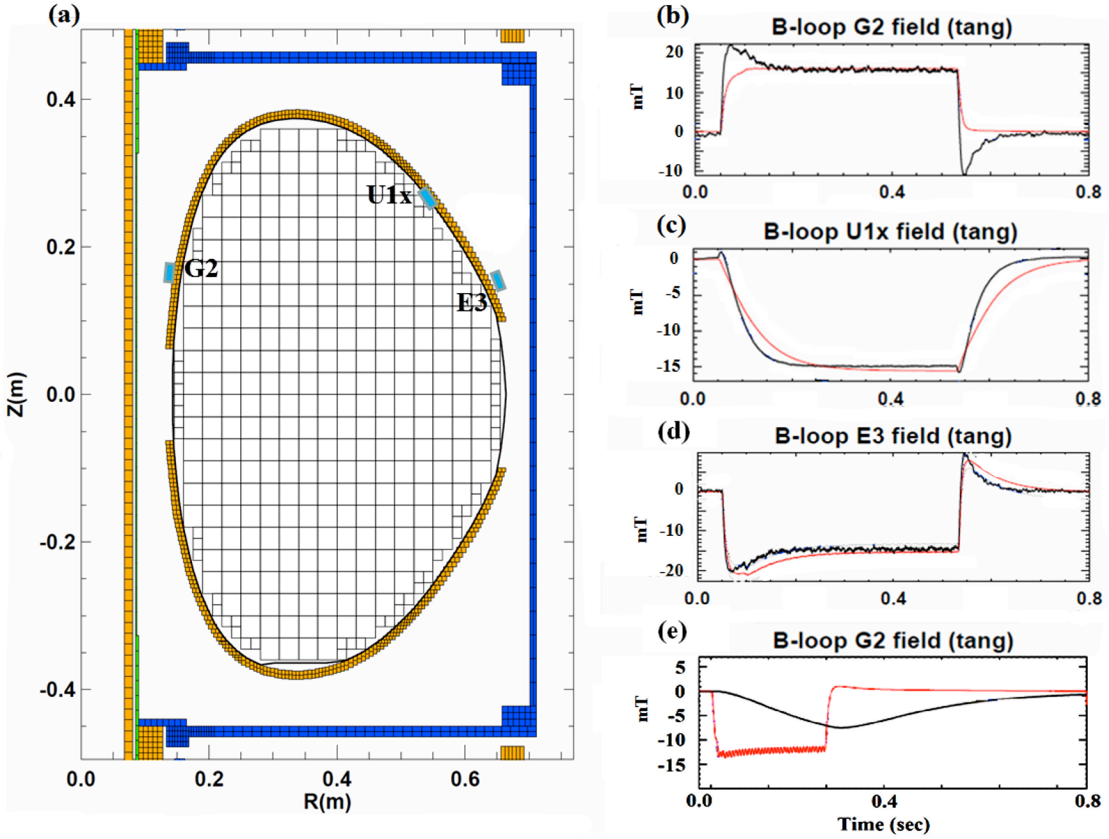

Figure 5: Comparison of LTX LRDFIT simulated and actual measured sensor signals for a poloidal field-only shot; (a) Sensor location of accompanying plots and shell elements in LTX LRDFIT model; (b)-(d) Plots of measured sensor signals (red) and simulated signals (black) as noted in titles. Agreement in the flattop region is to better than 2%; (e) Comparison of plot when no eddy currents are included in simulation, showing a lack of correspondence between measured and simulated signals.

LTX LRDFIT has been benchmarked against poloidal field-only pulses, where only the field coils generating poloidal fields are utilized, and there is no plasma present (figure 5). If eddy currents are not included in the simulation, a poor match between measured and simulated data occurs, as can be seen in figure 5(e), whereas a suitable match can be achieved when eddy current contributions are included (figure 5(b-d)). In addition, LTX LRDFIT has the ability to calculate eddy currents in the conducting structures themselves, and simulated currents have compared well to measurements of actual vessel eddy currents (figure 6).

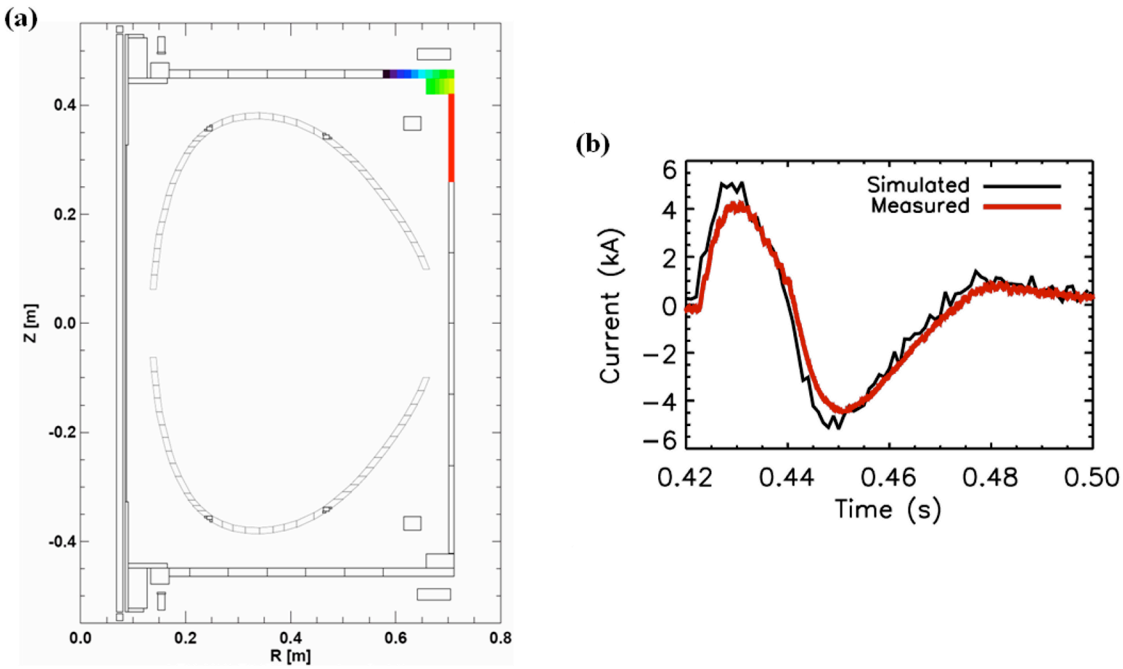

Figure 6: Comparison of simulated and measured eddy currents in the corner of the LTX vacuum vessel; (a) The coloured region is the approximate location of the Rogowski coil measuring vessel eddy currents and the region used in the simulation; (b) Simulated (black) and measured (thick red) current agree both temporally and in magnitude to better than 5%.

The ability to calculate and include eddy currents in simulations is a critical feature of LTX LRDFIT, making the code suitable for reconstructions of plasmas with discharge durations shorter than 10 ms and plasma currents lower than 15 kA (figure 7). For the SVD reconstructions, LRDFIT iteratively solves for the plasma toroidal current distribution, inside the limiter boundary, that provides a best fit to the magnetic diagnostic data when treating the coil currents and the circuit equations as known. The conducting regions allowed to carry toroidal plasma current are outlined in red in figure 4 and are enclosed by the limiter boundary as shown in black. Since the number of plasma current regions is generally much larger than the number of magnetic diagnostics constraining the SVD solution, a truncated SVD fit to the plasma current distribution is used, with typically 10-12 terms [13]. This number of terms is chosen to be sufficiently small such that the plasma current density distribution is smooth and of a single sign (i.e., the same sign as the total plasma current), and sufficiently large such that the fitting error becomes a slowly decreasing function of the number of terms kept [13].

3. Pre-lithium plasma discharges

In all new machines and machines which have undergone significant upgrades, it is necessary to develop a plasma start-up procedure. Achieving reliable start-up is greatly complicated by eddy currents in conducting structures which are closely coupled to the plasma, such as the non-axisymmetric eddy currents supported in the LTX shell structure. These non-axisymmetric eddy currents significantly alter the externally applied field structure inside the vessel, which correspondingly affects the design of the field null required for plasma start-up [7]. Iterative simulations using LTX LRDFIT, where simulated vacuum field plots were examined for regions of stable magnetic field, were critical in developing the poloidal and Ohmic field programming required for reliable LTX plasma start-up.

Once reliable plasma start-up was achieved in LTX, typical LTX discharges were low density (5 x 10^{18} m^{-3}), low current (~ 15 kA), and of short duration (~ 6 ms). However, even with the transient nature of early LTX discharges, LTX LRDFIT simulations converged for SVD reconstructions. These plasma flux surface reconstructions indicated the approximate plasma location as well as discharge evolution.

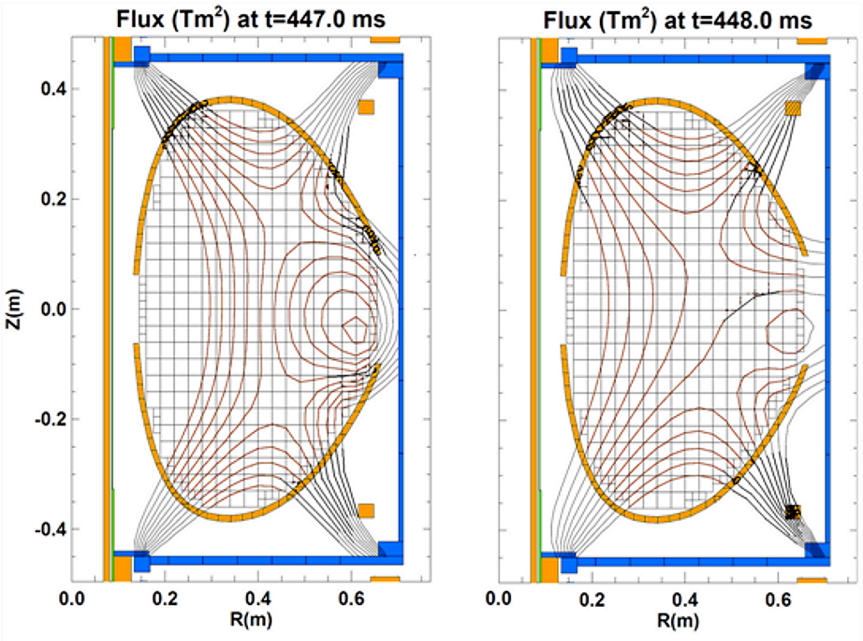

Figure 7: LTX LRDFIT reconstructions for a pre-lithium plasma. The plasma current extends from 444 ms to 448.3 ms with a peak of 7 kA from 446 ms to 447.5 ms. The plasma is vertically centered and outboard in the left reconstruction, and the plasma terminates outboard and on the lower shell in the right reconstruction.

Plasma reconstructions of these early discharges confirm nearly immediate plasma termination when a flux surface intersects a shell surface, as can be noted in the right image in figure 7. Extensive thermal wall conditioning procedures were utilized in order to enhance these early discharges. The shell quadrants were repeatedly heated to ~300 °C in order to evaporate water embedded in the shell surface. However, this plasma behavior is consistent with plasma termination caused by a sudden influx of impurities as the plasma strikes the shell. Early discharges were too short-lived to generate a repulsive, plasma-generated eddy current in the shell structure that would act to hold the plasma in a centered position. In place of this restoring force, significant eddy currents generated by the Ohmic pulse and circulating in the shell quadrants drive the plasma toward the shell and its subsequent termination.

4. Results from initial lithium wall conditioning

Although initially hindered by eddy currents, pre-lithium LTX discharges were optimized by minimizing the effect of undesired shell eddy currents. However, these pre-lithium discharges remained significantly limited by wall conditioning.

Initial lithium wall conditioning utilized two yttria crucibles loaded with lithium inserted into the vacuum vessel near the magnetic axis and separated toroidally by 180°. The yttria crucibles were heated to 580 °C and approximately 8 g of lithium was evaporated onto the shell quadrants. During evaporation, the vessel was backfilled with helium to a pressure of approximately 10 mTorr. The helium backfill permitted the evaporating lithium to be collisionally dispersed over the entire inner surface of the shells. Following an evaporation cycle, the residual gas analyzer (RGA) indicated an immediate, dramatic

decrease in impurities, particularly water, inside the vacuum vessel; there was approximately an order of magnitude reduction in the partial pressure of water to 1 x 10^{-8} T. The vessel base pressure is then dominated by hydrogen. Subsequent to this procedure, a dramatic improvement in plasma performance was immediately noted (figure 8 and figure 9).

Post-lithium discharges have more than 8 x 10^{18} m^{-3} line-averaged density, up to 67 kA plasma current, and 15-17 ms discharge duration (figure 8). Plasma reconstructions also show dramatic improvement in plasma centering and shaping (figure 10). The plasma position is significantly stabilized as compared to pre-lithium discharges, and plasma shaping is improved as the plasma grows conformally with the shell surface. Post-lithium plasmas are not destroyed by limiting on the shell surface and develop into stable discharges. This effect can be noted by comparing figure 7 and figure 10. Pre-lithium plasmas (figure 7) do not survive past the initial shell limited phase, while post-lithium plasmas (figure 10) develop and elongate off of the shell surface.

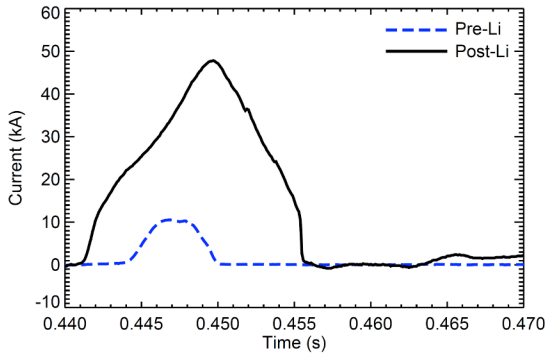

Figure 8 (Colour online): Comparison of plasma current between a pre- (blue dash) and post-lithium (black) discharge. The presence of lithium alters the start-up conditions, allowing post-lithium plasmas to initiate earlier than pre-lithium plasmas.

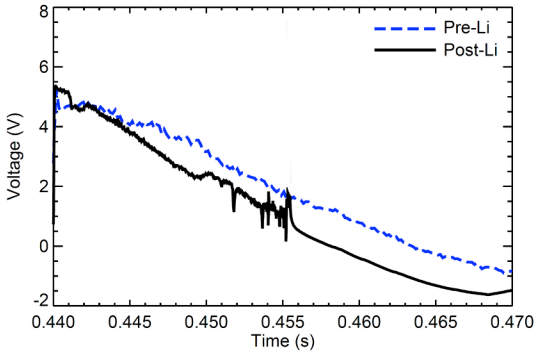

Figure 9 (Colour online): Comparison of loop voltage between a pre- (blue dash) and post-lithium (black) discharge. Although the magnitude of the loop voltage decays more slowly in the pre-lithium plasma shot, the plasma terminates more than 5 ms later when lithium is present.

5. Conclusions and future work

A closely coupled, conducting structure, such as the LTX internal shell quadrants, is required to investigate the effects of a lithium wall, but greatly complicates traditional plasma start-up and precludes

the usage of a standard equilibrium reconstruction code. LTX LRDFIT has been developed to address both of these challenges and has been used successfully for both. Plasma reconstructions are critical for determining the effect of the low-recycling, lithium wall on plasma performance, and LTX LRDFIT has been utilized to calculate and compare plasma flux surface reconstructions for pre- and post-lithium discharges.

A dramatic improvement in plasma performance has occurred with the introduction of initial lithium wall conditioning. Plasma current, density, and duration have all significantly increased, and plasma flux surface reconstructions indicate a stable, developing plasma.

Further calculations and LTX LRDFIT simulations are now required to ascertain the energy confinement time and the increase in plasma beta. With the flexibility of LTX LRDFIT and the success of the initial lithium wall conditioning, next steps for LTX will include introducing additional quantities of lithium and operating with a hot shell in order to generate a true liquid lithium wall.

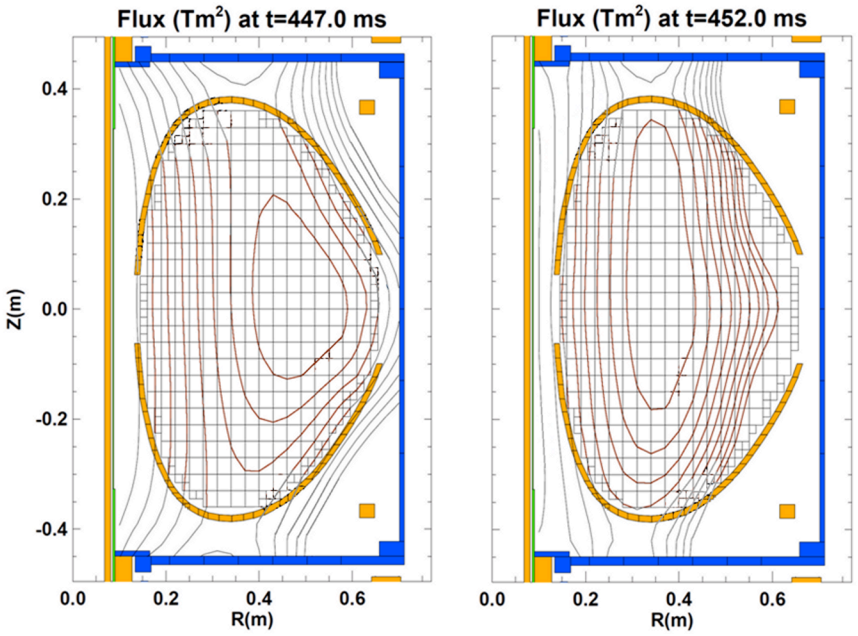

Figure 10: Plasma reconstructions of a representative post-lithium discharge. The plasma initiates at approximately 440 ms; the time stamps for these two reconstructions are near the peak in plasma current (~45 kA). The reconstructions indicate that the plasma is beginning to be shaped conformally to the shell, as designed, and that although the plasma limits on the upper shell, it is no longer immediately terminated.

Acknowledgements

This work is supported by US DOE contract DE-AC02-09CH11466.

The authors also wish to acknowledge the tireless efforts of the LTX technical staff, including Jim Taylor, and make a special acknowledgement of John Timberlake, who will be missed as part of the LTX team and whose wealth of knowledge and expertise was critical to the CDX-U and LTX lithium experiments.

References

[1] Majeski R et al. 2009 *Nuclear Fusion* **49**, 5

[2] Krasheninnikov S, Zakharov L and Pereverzev G 2003 *Physics of Plasmas* **10**, 1678

[3] Majeski R, Boaz M, Hoffman D, Jones B, Kaita R, Kugel H, Munsat T, Spaleta J, Soukhanovskii V and Timberlake J 2003 *Journal of Nuclear Materials* **313-316**, 625

[4] Kaita R et al. 2002 *Fusion Engineering and Design* **61-62**, 217

[5] Majeski R, Doerner R, Gray T, Kaita R, Maingi R, Mansfield D, Spaleta J, Soukhanovskii V, Timberlake J and Zakharov L 2006 *Physical Review Letters* **97**, 075002

[6] Berzak L, Jones A, Kaita R, Kozub T, Logan N, Majeski R, Menard J and Zakharov L 2010 *Review of Scientific Instruments* **81**, 10E114

[7] Berzak L 2010 *Plasma start-up in a spherical tokamak with close-fitting conducting walls* (Princeton University PhD dissertation)

[8] Berzak L, Kaita R, Kozub T, Majeski R and Zakharov L 2008 *Review of Scientific Instruments* **79**, 10F116

[9] Menard J, Bell R, Gates D, Kaye S, LeBlanc B, Levinton F, Medley S, Sabbagh S, Stutman D, Tritz K and Yuh H 2006 *Phys. Rev. Lett*. **97**, 095002

[10] Grover F 1946 & 1973 *Inductance Calculations – Working Formulas and Tables* 2004 edn (New York: Dover Publications) eqn 99

[11] Terman F 1943 *Radio Engineer's Handbook* (New York: McGraw-Hill) pg 72

[12] Snow, C 1953 *Magnetic Fields of Cylindrical Coils and Annular Coils* (National Bureau of Standards Applied Mathematical Series 38)

[13] Hansen, P C 1990 *SIAM J. Sci. Stat. Comp.* **11**, 503-518

The Princeton Plasma Physics Laboratory is operated
by Princeton University under contract
with the U.S. Department of Energy.

Information Services
Princeton Plasma Physics Laboratory
P.O. Box 451
Princeton, NJ 08543

Phone: 609-243-2245
Fax: 609-243-2751
e-mail: pppl_info@pppl.gov
Internet Address: http://www.pppl.gov